THE ASTROPHYSICAL JOURNAL, 456:708–716, 1996 January 10

ON THE NONLINEAR EVOLUTION OF MAGNETOHYDRODYNAMIC KELVIN-HELMHOLTZ INSTABILITIES

ANDREA MALAGOLI
EFI/LASR, University of Chicago, 933 E. 56th Street, Chicago, IL 60637
GIANLUIGI BODO
Osservatorio Astronomico di Torino, Strada Dell'Osservatorio 20, Pino Torinese, 10025, Italy
AND
ROBERT ROSNER
EFI/LASR, University of Chicago, 933 E. 56th Street, Chicago, IL 60637
Received 1995 April 10; accepted 1995 July 19

ABSTRACT

We investigate the physical behavior in the nonlinear regime of Kelvin-Helmholtz (KH) instabilities in a simple conducting shear flow in the presence of magnetic fields, based upon the use of numerical simulations of the ideal magnetofluid equations of motion in two dimensions. The flow is characterized by three principal control parameters: the Mach number M of the shear flow, the ratio α of the Alfvén speed to the sound speed, and the effective diffusivity; we investigate how these parameters affect the evolution and saturation of the instability. The key result of our study is that even relatively small magnetic fields (i.e., small compared to the equipartition intensity) affect the way the KH instability saturates with respect to the purely hydrodynamic case. If the magnetic field intensity is not sufficiently strong to suppress the KH instability entirely, then the field itself can still mediate the turbulent decay and diffusion of energy and mass across the layer. We present a detailed study of the various phases of this process for our simple shear layer configuration.

Subject headings: instabilities — methods: numerical — MHD — plasmas

1. INTRODUCTION

The instability of the boundary layer separating two fluids in relative motion (Kelvin-Helmholtz instability) appears frequently in many astrophysical and geophysical situations, ranging from the interaction of the solar wind with the magnetospheric boundary (Uberoi 1984) and cometary tails (Ray 1982) to the dynamics of accretion disks (Anzer & Börner 1983) and jets in extragalactic radio sources (Birkinshaw 1991a) and young stellar objects (Bührke, Mundt, & Ray 1988). Many studies have therefore been devoted to understanding the linear behavior of the instability under the influence of different physical ingredients typical of these widely differing environments. Starting from the classical results for the incompressible case, which can be found summarized in Chandrasekhar's monograph (1961), the effects of compressibility have been introduced both in the pure hydrodynamical situation (Sen 1964; Gerwin 1968) and in the magnetohydrodynamic (MHD) case (Sen 1963; Pu & Kivelson 1983). The effect of a finite thickness of the shear layer has been discussed by Ray (1982) and Ferrari & Trussoni (1983). The case of cylindrical geometry, which applies to astrophysical jets, has been studied by Ferrari, Trussoni, & Zaninetti (1981), while the extension to relativistic velocities, again in relation with extragalactic jets, has been considered by Ferrari, Trussoni, & Zaninetti (1980) and by Birkinshaw (1991b). Finally, the effects of anisotropic pressure, typical, for example, of CGL theory, have been analyzed by Trussoni et al. (1988).

More recently, thanks to a wider availability of supercomputers (and of sufficient computing time to solve large problems) and to the development of refined algorithms for the solution of fluid equations, it has been possible to begin the analysis of the evolution of the instability in the fully nonlinear regime. The pure hydrodynamical case has been widely investigated (see, e.g., Woodward 1987; Lele 1989; Sandham & Reynolds 1989, 1991), while only few results have been obtained for the MHD cases; this lag in the MHD cases has occurred because of the greater difficulty in finding accurate and robust algorithms for the solution of the MHD equations. Thus, Miura (1984) investigated the evolution of a single shear layer with a uniform magnetic field either parallel or perpendicular to the direction of the flow; however, his results are limited in the exploration of the parameter space and in the extent of time during which the evolution is followed. Finally, Hardee et al. (1992) have studied the evolution of a double shear layer with a uniform longitudinal magnetic field and a supersonic flow velocity. The focus of their work is, however, more on the comparison between the scale length of the structures generated during the nonlinear evolution and the wavelengths of maximum growth rate predicted by the linear theory than on the new physical effects introduced by the magnetic field.

Recently, Zachary, Malagoli, & Colella (1994) have developed a MHD code based on a high-order Godunov method. Methods of this kind have, in fact, proven to be very effective for supersonic flows in the hydrodynamical case. In this paper we describe the results obtained for the evolution of two-dimensional perturbations of a single planar shear layer obtained with this code.

The introduction of magnetic fields can be expected to introduce several new physical effects that may change the evolution of the instability significantly with respect to the purely hydrodynamic case. For example, we recall that in two-dimensional hydrodynamical turbulent flows, there is an inverse cascade of energy toward small wavenumbers, whereas in the three-dimensional case, the cascade of energy is toward large wavenumbers; in contrast, the cascade of energy is always toward small wavelengths in the MHD case, even in

two dimensions (Pouquet 1978; Orszag & Tang 1979; Biskamp & Welter 1983). As a second important effect, we observe that energy can be dissipated via magnetic field reconnection as well as via viscosity (Frisch et al. 1983; Biskamp & Welter 1983). In this paper we analyze how these new physical effects affect the simplest nontrivial shear flow configuration, namely, a single shear layer with a uniform field directed along the flow. Furthermore, we restrict our attention to relative velocities near Mach number $M = 2V_0/c_s = 1$ (where c_s is the sound speed); this restriction is based on the fact that for supersonic velocities it is known that the nature of the linear instability changes from monotonic to oscillatory and that new nonlinear instabilities appear (see discussion below). This supersonic case will be the subject of a subsequent paper.

The organization of this paper is as follows: in § 2 we describe the physical problem we study, summarize the basic results in linear theory, and outline the numerical method used for the integration of the MHD equation; we describe our results in § 3. Section 4 is devoted to the summary and discussion.

2. THE PHYSICAL PROBLEM

2.1. *Basic Equations and Initial Configurations*

We study the nonlinear evolution of the Kelvin-Helmholtz instability of a single magnetized planar velocity shear layer. The relevant equations are the compressible single-fluid MHD equations:

$$\frac{\partial \rho}{\partial t} + \nabla \cdot (\rho \boldsymbol{v}) = 0 , \tag{1}$$

$$\frac{\partial (\rho \boldsymbol{v})}{\partial t} + \nabla \cdot \left(\rho \boldsymbol{v} \cdot \boldsymbol{v} - \frac{1}{4\pi} \boldsymbol{B} \cdot \boldsymbol{B} + p + \frac{1}{8\pi} B^2 \right) = \mu_{\rm visc} , \tag{2}$$

$$\frac{\partial \boldsymbol{B}}{\partial t} + \nabla \cdot (\boldsymbol{v} \cdot \boldsymbol{B} - \boldsymbol{B} \cdot \boldsymbol{v}) = \beta_{\rm res} , \tag{3}$$

$$\frac{\partial \rho E}{\partial t} + \nabla \cdot \left[\rho \boldsymbol{v} E + \boldsymbol{v} p - \frac{1}{4\pi} \boldsymbol{B} (\boldsymbol{B} \cdot \boldsymbol{v}) \right] = \epsilon_{\rm visc} + \epsilon_{\rm res} , \tag{4}$$

$$E = \frac{1}{2} v^2 + \frac{1}{\gamma - 1} \frac{P}{\rho} + \frac{B^2}{8\pi\rho} , \tag{5}$$

in Cartesian geometry, where the variables E, p, ρ, $\boldsymbol{v}$, and $\boldsymbol{B}$ are, as customary, the specific energy, pressure, density, velocity, and magnetic field, respectively, and γ is the ratio of the specific heats. Here we do not give the specific expression for the viscous and dissipative terms $\mu_{\rm visc}$, $\beta_{\rm res}$, $\epsilon_{\rm visc}$, and $\epsilon_{\rm res}$ that appear in the momentum, induction, and energy equations. In our code, these terms are not introduced explicitly but arise from the complicated numerical dissipation mechanism of the Godunov method, for which there is no analytic expression. We will discuss the rationale for these terms in § 2.3. For the moment, we simply assume that these terms are very small, so that they do not need to be included in the linear instability analysis. However, we will see that the nonlinear saturation of the Kelvin-Helmholtz instability does require the presence of viscous and resistive dissipation.

In the initial configuration, the fluid moves with a velocity v_x, which has the shear profile along the y-direction

$$v_x = V_0 \tanh (y/a) , \tag{6}$$

and the other quantities are uniform. In particular, the uniform magnetic field is directed along the x-direction, parallel to the velocity. We now impose a perturbation to the y component of the velocity at $t = 0$ of the form

$$v_y = v_{y,0} \sin (k_x x) \exp [-(y/\sigma)^2] , \tag{7}$$

where $v_{y,0} (\ll V_0)$ is the amplitude of the initial perturbation, k_x is its wavenumber along the x-direction, and σ is a parameter that fixes its width along the y-direction.

The numerical calculations will be performed on a domain of size $D = 2\pi/k_x$ in the longitudinal x-direction and $2D$ in the transverse y-direction. We take D as our unit of length and the Alfvén crossing time over D, $\tau_A = D/v_A$, as our unit of time (v_A is the initial Alfvén velocity). In general, a and σ should be chosen to satisfy $h < a \ll D$, where h is the size of the computational grid cells and $\sigma < D$, but their specific values are not expected to influence our results. The reason for the choice of a is dictated by numerical considerations, as discussed below, while σ simply makes sure that the perturbation amplitude decays away from the vortex sheet. Here we have chosen $a = D/20$ and $\sigma = D/10$. We assume periodicity in the longitudinal direction, thus imposing periodic conditions at the longitudinal boundaries; free outflow conditions are used instead at the outer boundaries, viz., at $y = \pm D$.

2.2. *Linear Results*

The linear stability properties of a magnetized velocity shear configuration have been extensively studied by many authors, starting with the early work of Chandrasekhar (1961) on the incompressible vortex sheet case. The effects of compressibility have been taken into account by Sen (1964), Fejer (1964), Talwar (1964), Southwood (1964), and Pu & Kivelson (1980); the effects of a smooth velocity shear layer (as opposed to the vortex sheet assumed in earlier linear analyses) have been considered by Lau & Liu (1980), Ferrari & Trussoni (1983), and Miura & Pritchett (1982).

The main effect of the magnetic field on the flow stability properties is to stabilize the fluid interface with respect to the pure hydrodynamic case; this effect can be understood simply as the consequence of field line tension, quite analogous to the stabilizing role played by surface tension in the context of Rayleigh-Taylor instability. The resulting decrease in growth rates is a sensitive function of the field strength, and full stability is reached when the Alfvén velocity becomes of the order of the total velocity jump across the shear layer. The condition $V_0 > v_a$ for instability holds exactly in the simpler incompressible vortex sheet case; in the compressible case, in which one also allows for the effects of a finite width shear layer, this condition is only approximately valid (Pu & Kivelson 1980; Lau & Liu 1980).

Compressibility has the principal effect of introducing a high Mach number cutoff to the instability: although in the incompressible case, instability is found for every value of the velocity jump, a compressible vortex sheet is unstable only for $M < M_c$, where M_c is a critical value that depends on the fast magnetosonic velocity. This behavior is analogous to that of the pure hydrodynamical case, in which stability occurs for $M > 2\sqrt{2}$. As for that case, a smooth layer is unstable also for $M > M_c$ if we remove the requirement that perturbations vanish at infinity and allow for radiation boundary conditions (Blumen et al. 1975; Ferrari & Trussoni 1983). It is also well known (see Artola & Majda 1988, 1989a, b) that in this high Mach number regime, nonlinear instabilities develop that have a very different evolution from the nonlinear counterpart of the

Kelvin-Helmholtz instability, although they also ultimately lead to the growth of a mixing layer.

Finally, the introduction of a smooth shear layer has also a stabilizing effect on small-wavelength perturbations. Contrary to the vortex sheet case, which was a scale-free problem, we have here a defined scale, i.e., the thickness of the shear layer, which is chosen so that there are at least five computational cells within the shear layer. In the scale-free case, the growth rate was proportional to the wavenumber k; this behavior is still valid for the smooth shear layer in the low-wavenumber (large wavelength compared to the thickness) regime. As the wavenumber is increased, the growth rate reaches a maximum at $ka \sim 1$ and then decreases, reaching stability for values of $ka \sim 2$, with the exact value depending on the other parameters (Ferrari & Trussoni 1983; Miura & Pritchett 1982; Ray 1982). The main reason for the introduction of a finite thickness of the shear layer is precisely to stabilize very short wavelengths with a scale comparable to the size h of the computational cells: although these wavelengths are near the dissipation scale of the numerical code and would probably be damped, they sometimes introduce large spurious oscillations in the simulations. Since we are primarily interested in the large-scale features of the flow, with low-wavenumber modes $k \ll 1/a$, this does not represent a problem.

2.3. *The Numerical Method*

We have used here for the first time the new multidimensional code for ideal magnetohydrodynamics developed by Zachary et al. (1994). This code is a higher order Godunov method that uses an approximate Riemann solver for ideal MHD. Higher order Godunov methods have been used successfully to study problems in compressible hydrodynamics, which involve the formation and evolution of strong shock discontinuities. The most prominent representative of this class of codes is certainly the piecewise parabolic method of Colella & Woodward (1984), which has been used extensively to study a wide variety of problems in astrophysical fluid dynamics, ranging from supersonic compressible convection (Malagoli et al. 1991; Porter et al. 1994) to supernovae explosions (Fryxell et al. 1991). Our MHD code reconstructs the profiles of the physical variables using piecewise linear interpolation, followed by projection onto characteristics for the construction of the left and right states at the cell boundaries. The most delicate and interesting part of the method is its approximate Riemann solver. Contrary to the hydrodynamic case, the Riemann problem for ideal MHD does not have a completely consistent and unique solution because the MHD equations are not strictly hyperbolic, in the sense that characteristics can become degenerate, depending on the orientation of the magnetic field. As a consequence, it is not possible to give a general formulation for Lax's entropy condition (Lax 1954). Our Riemann solver is based on the Engquist-Osher flux formulation given by Bell, Colella, & Tragenstein (1982), plus several switches that treat the special cases of characteristic degeneracies. The resulting code has proven stable and robust on a large test suite of problems (see Zachary et al. 1994).

Although we are trying to solve a problem that is very close to the ideal MHD limit because of the very small dissipation present in astrophysical plasmas, numerical dissipation cannot be avoided; typically, such numerical dissipation is much larger than physical diffusion for the grid sizes allowed by current (and anticipated) computer hardware. As we have done in the past (see, e.g., Bogdan et al. 1993), we assume that the dissipation mechanism of the Godunov method provides an adequate model for subgrid-scale dissipation, while ensuring the highest possible resolution, i.e., lowest possible dissipation, for a given grid size. Our and others' (Porter et al. 1994; Boris 1991) experience suggests that the numerical dissipation of monotonic schemes can indeed be used as a reasonable model for subgrid-scale dissipation. For more quantitative evidence, we have simulated the turbulent decay of a magnetized Orszag-Tang vortex (Orszag & Tang 1979) with our code and have found that the results are in good agreement with those from a pseudospectral code with physical dissipation taken into account (Picone & Dahlburgh 1991; however, our calculation required fewer grid points). Our assumption is even more reasonable in the case of astrophysical plasmas, where fundamental uncertainties in the observations will make any phenomenological dissipation model equally uncertain, even if it were based on more theoretically motivated considerations than purely numerical effects. Ultimately, we will use our physical intuition and our experience with the numerical algorithm to evaluate and analyze the results from the numerical experiments, in a way similar to laboratory experiments.

3. RESULTS

In this paper, we have focused on the case of a marginally supersonic shear layer, i.e., on the case in which the relative shear velocity reaches at most $M = 1$ (the case of strongly supersonic flows will be treated in a subsequent paper). We have varied the relative Mach number between $M = 0.5$ and $M = 1$, but we will discuss only this last case since we obtain essentially the same results for $M = 0.5$. In addition, we have varied the relative strength of the initial magnetic field $|\boldsymbol{B}_0|$, as measured by the ratio $\alpha \equiv v_A/c_s$, between $\alpha = 0.05$ and $\alpha = 0.25$ ($\alpha_c = 0.5$ being the critical value above which the flow is linearly stable). Finally, we have repeated one case, namely, $M = 1$ and $\alpha = 0.1$, using two different grid resolutions (100×200 and 256×512) in order to estimate the effects of decreasing the effective dissipation. Some of the cases we consider are essentially identical to those studied by Miura (1984), although our calculations achieve higher resolution and are carried out for longer times. As we shall see, both differences lead us to modify some of Miura's conclusions substantially.

We have identified three stages in the evolution of the shear layer instability; we discuss these in turn immediately following.

Phase 1: The initial phase strongly resembles the evolution expected for the ideal MHD problem in the linear regime, in which the instability grows exponentially; the leftmost panel in Figure 1 displays a gray-scale snapshot of the fluid density during this phase and shows the characteristic vortical pattern traditionally associated with the hydrodynamic Kelvin-Helmholtz instability. This phase is also characterized by growth of the magnetic field, which is frozen into the fluid and is therefore stretched by the vortical motions.

The initial topology of the magnetic field line stretching is illustrated in the top two panels of Figure 2. We follow two field lines located symmetrically on both sides of the shear layer. The field lines are expelled from the center of the initial large vortices and are stretched into narrow filaments, which turn out to be slow magnetosonic waves (in fact, rarefaction waves). The magnetic field strength is concentrated and amplified inside these slow waves, until localized reconnection events occur (bottom panel of Fig. 2), thus ending the ideal MHD phase of the evolution.

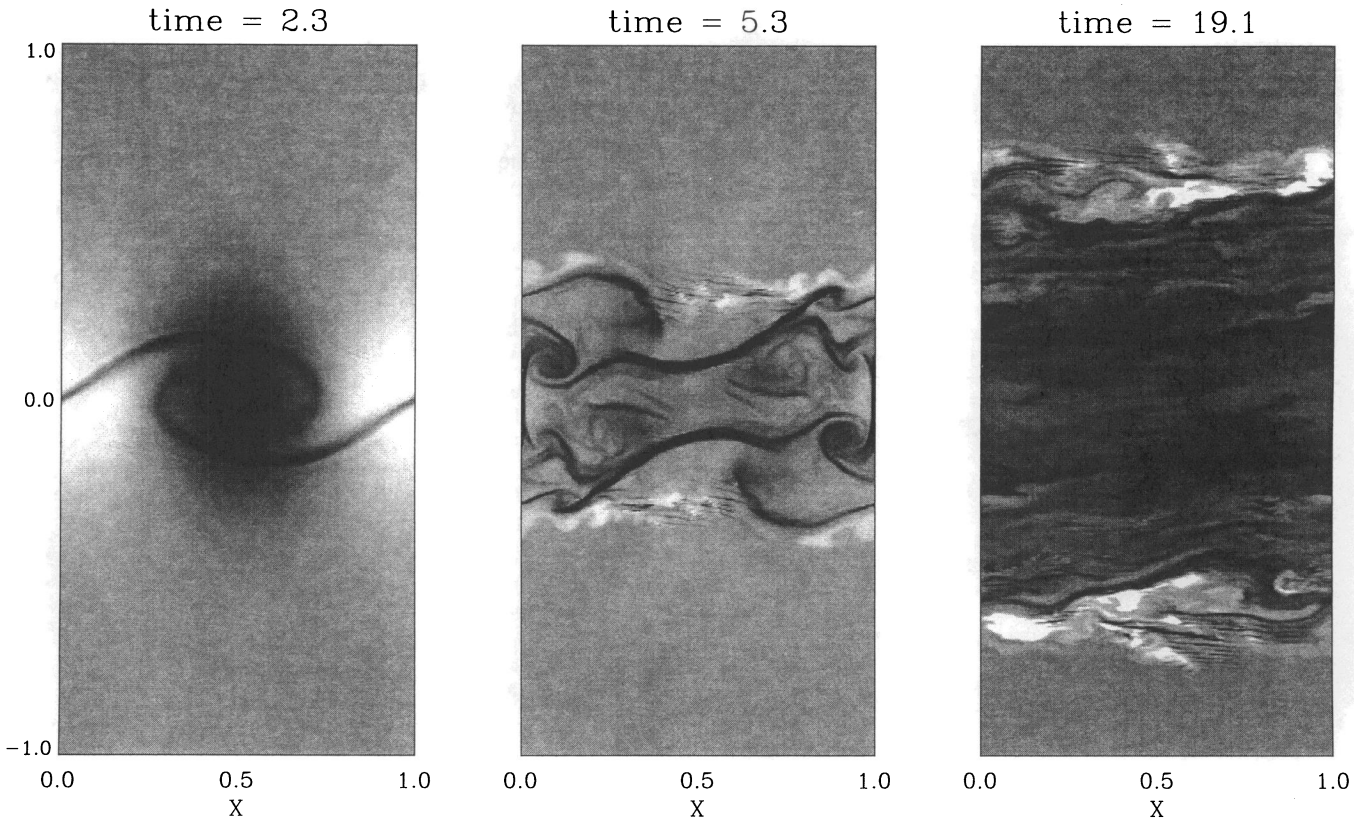

FIG. 1.—The leftmost panel shows a gray-scale snapshot of the fluid density during phase 1 (time $T = 2.3$). Denser regions are white, and emptier (rarefied) regions are black. The spiral pattern of less dense matter corresponds to the slow rarefaction wave discussed in the text. The wavelength of the initial perturbation is $\lambda = 1$. The middle panel shows the density field during phase 2 (time $T = 5.3$), in which strongly turbulent fluid motions are produced by the transient reconnection events. The rightmost panel shows the fluid density during phase 3 (the final phase $T = 19.1$). The case shown has $M = 1$ and $\alpha = 0.1$.

It is essential to realize that the field amplification observed during this phase *cannot* be a dynamo process. It has been long recognized that in two dimensions, regenerative dynamo action is impossible in principle (see Moffatt 1978, and references therein). Thus, the amplification we observe must be a transient phenomenon, and one would then expect that the field will eventually decay, once the instability saturates, owing to resistive dissipation; this is indeed what we subsequently observe (see below). In this context, it is useful to note that Miura (1984)'s calculations terminated during this phase, in which strong field amplification was also observed by him; indeed, Miura concludes that the KH instability constitutes a dynamo process on the basis of this observed magnetic field amplification. It should now be clear that this conclusion was premature.

Phase 2: As the magnetic field is stretched by the vortical flows, the gradient scales of the magnetic field go to smaller and smaller scales; this process is observed to continue until the field gradient scales are of order the resistive dissipation scale in the calculation (given approximately by the grid spacing for our code), at which point resistive reconnection takes place, and small-scale turbulent motions develop. At this time, the magnetic energy reaches its maximum value and decays subsequently. The middle panel of Figure 1 shows a snapshot of the density during this phase. The filamentary structures in the density distribution closely trace filaments of strong magnetic field concentration.

The process by which magnetic field decay occurs is seen in the sequence of contour plots shown in Figure 3: viz., the magnetic field begins to reconnect. However, this reconnection process proceeds initially in an intermittent manner. That is, after each reconnection event that leads to field decay smaller scale vortex motions develop, which in turn "rewind" and strengthen the magnetic field until new (smaller scale) magnetic structures are generated, which then in turn again decay by reconnection and thereby release further energy. This process, which is a well-known feature of MHD turbulence (see, e.g., Biskamp & Welter 1983), leads to a cascade of both energy and enstrophy to smaller and smaller scales. Figure 4 illustrates this behavior: the maximum in magnetic energy coincides temporally with the first reconnection event seen in Figure 3; immediately subsequent to this event, one can see the magnetic energy build up once more (although not to as high a peak value as in the first instance), only to decay yet again as the newly formed smaller scale field structure reconnects.

An obvious question is how these results depend on the effective resistivity, or equivalently on the grid resolution of the calculation. In particular, we can ask how the field amplification is modified by the decrease in resistivity (i.e., by an increase in resolution). In order to answer this question, we have run a problem with the same parameters on two distinct grid sizes (100 × 200 and 256 × 512) and computed two quantities: first and most obvious, the total magnetic energy; second, the smallest spatial scale associated with the magnetic field perturbations, as measured by $\lambda \equiv \min(|\boldsymbol{B}|/|\nabla \times \boldsymbol{B}|)$. Figure 5 shows the evolution of the two quantities for the two cases. As expected, at the higher magnetic Reynolds number, which corresponds to the higher grid resolution, diffusive

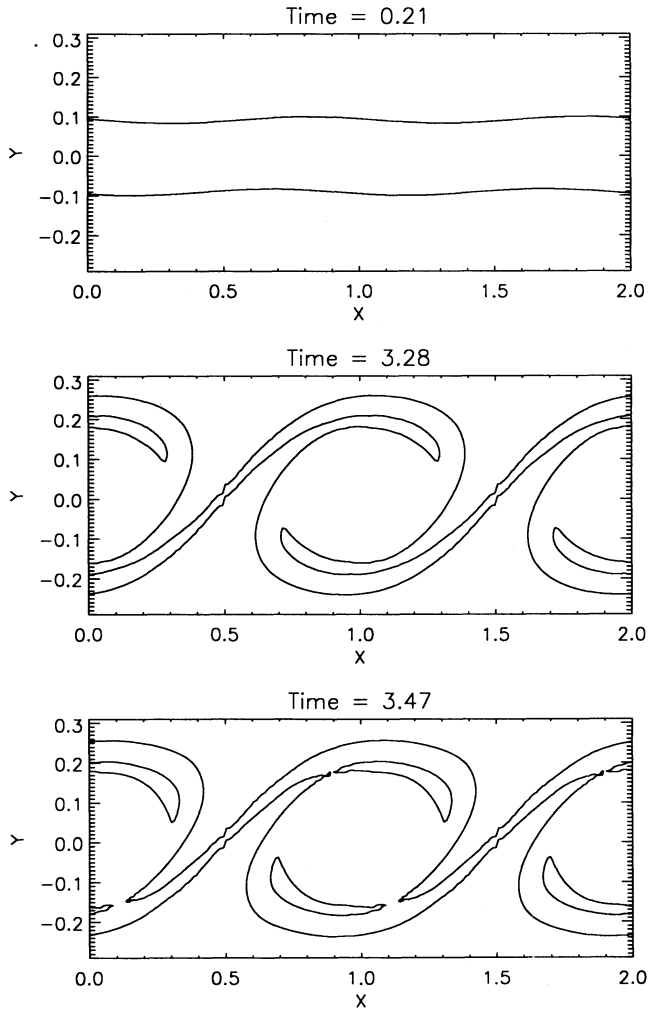

FIG. 2.—Contour plots of selected magnetic field lines during phases 1 and 2 of the instability evolution. The upper panel displays these field lines during the very initial period of phase 1; the middle panel illustrates the wrap-up, or stretching, of field lines during the course of phase 1; and the lower panel shows the onset of phase 2, in which magnetic field lines wrapped up by the vortical fluid motions begin to reconnect and thereby dissipate magnetic energy.

scales are smaller. As a consequence, the magnetic field lines are distorted to smaller scales, namely, all the way down to the smaller diffusive scales, and the resulting field amplification is larger: the total magnetic energy grows to a higher maximum for the higher grid resolution.

One can also ask how the results depend on the strength of the initial magnetic field in the shear layer; one expects that for sufficiently strong magnetic fields, the instability ought to be suppressed. Figure 6 shows the results of a parameter study of this question as a function of $\alpha \equiv v_A/c_s$. Our results confirm our expectations: while the temporal evolution of the magnetic field is not especially sensitive to α for smaller values of α (i.e., for weak initial magnetic fields), there is a sudden transition in which significant field amplification and the instability itself are suppressed when α becomes larger than a critical value (here roughly 0.1). For $\alpha < 0.1$ the stretching of the magnetic field (and the corresponding amplification of the field's strength) is limited by the formation of field structures at the smallest possible scale, i.e., at the resistive diffusion scale. This effect is shown in the lower panel in Figure 6, which displays the time evolution of λ, which can be taken as a measure of the size of the smallest magnetic field structure. This means that the field amplification, as measured by the ratio $\int d^2x B^2(t)/\int d^2x B_0^2$, is independent of the initial strength $|B_0|$, as can be seen from the upper panel of Figure 6. For $\alpha > 0.1$ all of these effects, particularly the formation of small-scale field structures, gradually decrease until the instability is eventually completely suppressed (for $\alpha \sim 0.2$).

Finally, we note that this phase is also characterized by a rapid increase in the shear layer width, and hence in mixing across the shear layer, as indicated in Figure 7. This mixing is driven by the small-scale turbulent motions seen in, for example, the middle panel in Figure 1 (which is a snapshot taken during this phase). Figure 7 also shows that the widening of the shear layer reaches an asymptotic quasi–steady state, which turns out to signal the onset of phase 3, discussed next.

Phase 3: In the final phase, the small-scale turbulence decays monotonically until a new statistically steady flow sets in. The final result is the formation of an enlarged, mixed layer that exhibits filamentary structures approximately elongated along the direction of the initial shearing flow, and aligned with the magnetic field. The rightmost panel of Figure 1 is a snapshot of this final phase.

The formation of filamentary aligned structures is a known feature of decaying, magnetohydrodynamic turbulence and has been observed previously by, for example, Picone & Dahlburgh (1991). Once the alignment process occurs, further destabilization of the shear layer seems to cease altogether, and, in concert, further widening of the shear layer and magnetic field decay also cease. The result is an asymptotically stable shear flow, as seen in the final state in the rightmost panel of Figure 1. The mean flow velocity assumes a quasi-linear profile across the shear layer, as shown in Figure 7, and, in the central parts of the layer, fluid motions cease almost completely. The final layer is slightly hotter than the surrounding fluid, as a result of the dissipative heating that occurs during the decay of small-scale turbulence. This can be seen in Figure 8: since the layer is again in gas pressure equilibrium with the surrounding medium, the heating of the fluid has caused the layer to expand, thus lowering the density in the center.

We conclude that the evolution of the shear flow instability in the magnetized fluid case is indeed distinctly different than in the purely hydrodynamic case. Most prominently, the basic mechanism for the saturation of the instability in the magnetic case is a transfer of kinetic to magnetic energy (phase 1), followed by its dissipation via magnetic reconnection (phases 2 and 3). Contrary to the purely hydrodynamic case, in which energy cascades toward the largest scales and vorticity concentrates into a single isolated vortex, here energy can cascade to small scales, where it is dissipated, and vorticity is uniformly redistributed (rather than concentrated) over a final, wider shear layer. The typical timescale of the entire process is of the order of a few Alfvén crossing times. The width of the final layer is of the same order as the initial perturbation wavelength for the weaker initial magnetic fields ($\alpha < 0.1$); it gradually decreases as α is increased, as is to be expected as a consequence of the weakening of the instability (cf. Fig. 9). The material within the layer is completely mixed, but there is no substantial loss of mass from the layer: this result, which can be trivially inferred by looking at Figures 1 and 2, has also been confirmed by looking at the dispersion of a passive scalar field by this shear flow.

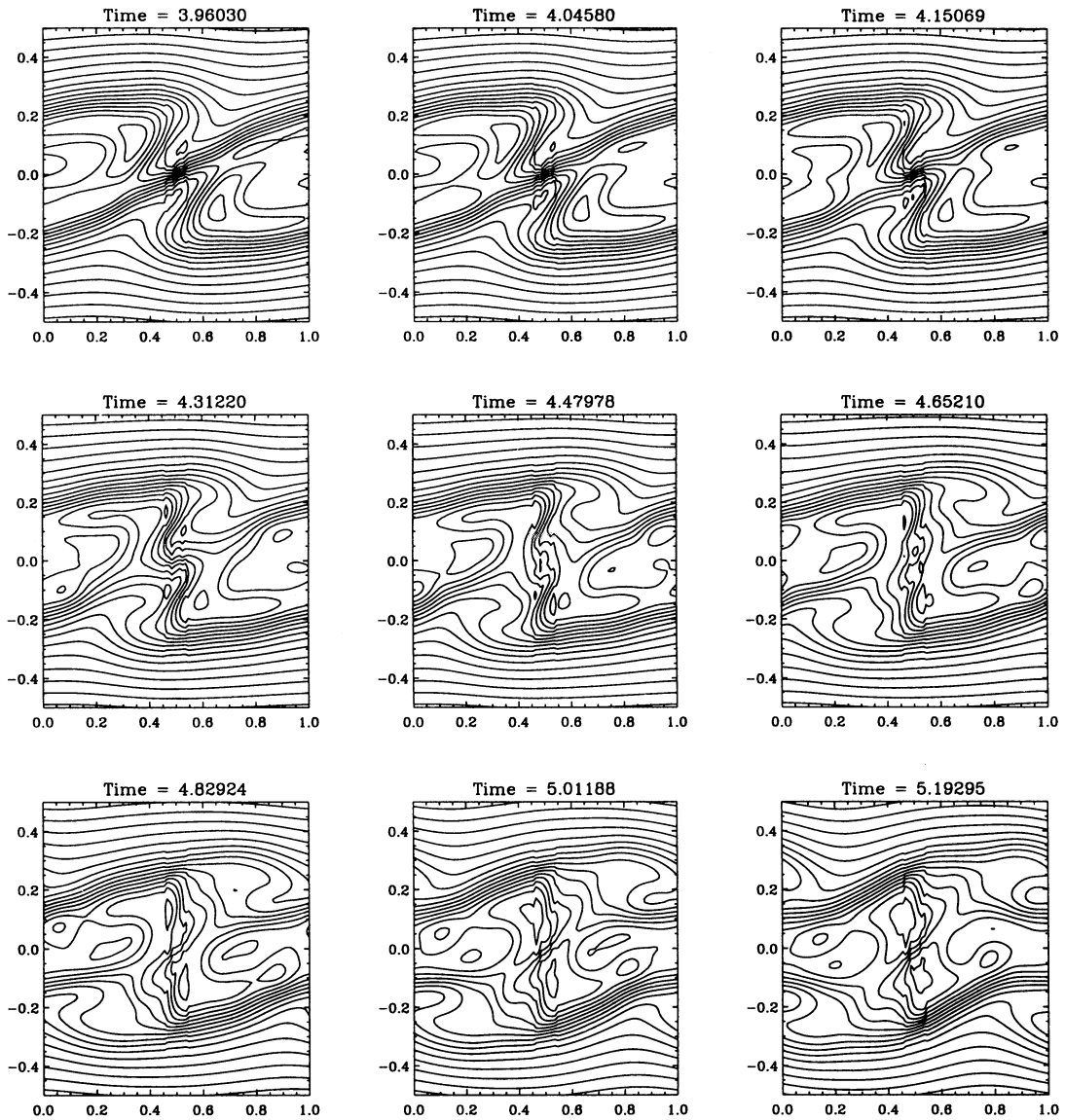

FIG. 3.—Snapshots in time of magnetic field line plots, taken from the same calculation as in Fig. 1 (at the lower resolution); time runs from left to right, and top to bottom (the time at which each snapshot is taken is indicated at the top of each panel). One can clearly see the reconnection event at $t \sim 4$ and the reformation of a smaller scale vortex at $t \sim 5.01$; they are a succession of such events (marked in Fig. 3 by the two peaks in the magnetic energy temporal evolution) that terminate the "ideal" phase of the instability.

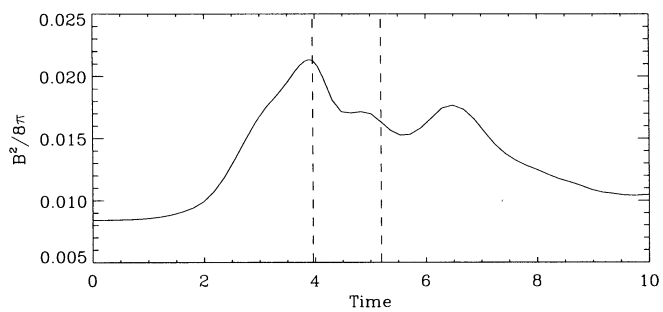

FIG. 4.—Evolution of the average magnetic energy for the same calculation as in Fig. 1 (at the lower resolution). The dashed vertical lines delimit the time interval in which the snapshots of Fig. 3 are taken. One can see how the occurrence of reconnection events that end the "ideal" phase of the instability is also marked by the beginning of the magnetic field decay.

One question might be whether our choice of the initial perturbation is in any way restrictive, since the perturbation wavelength used in the calculations has been chosen to be much larger than the thickness of the layer ($ka = 0.05$), which is much larger than the wavelength of the fastest growing mode ($ka \sim 1$). We believe that the answer is no, and our reasoning is as follows: The hydrodynamical results tell us that long-wavelength modes dominate the evolution past the linear stage. The reason is that although short-wavelength perturbations grow faster in the linear stage, they readily transfer energy to longer wavelengths through the vortex pairing process in the nonlinear regime. In the magnetic case we expect to follow this hydrodynamic scenario during our phase 1 (i.e., before the field becomes dynamically important); thus, we expect the largest wavelength excited mode to dominate at the

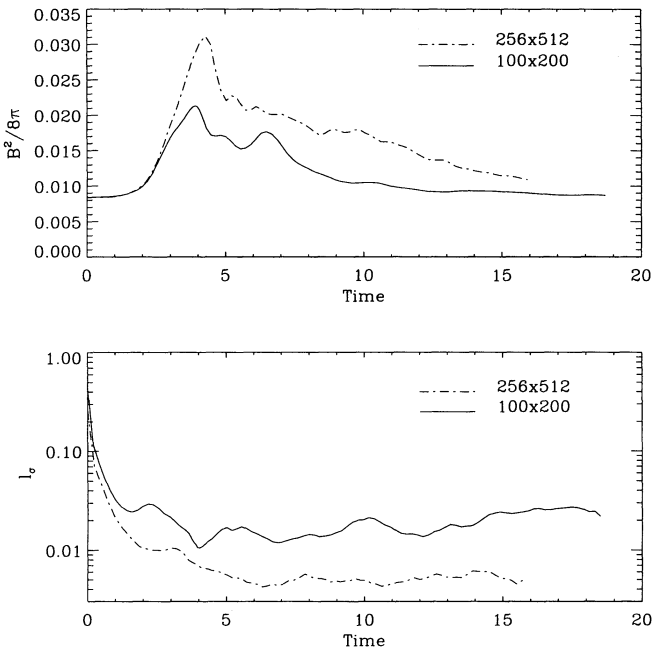

FIG. 5.—Magnetic field evolution as a function of effective resistivity, or grid resolution. The upper panel shows the averaged magnetic energy; the lower panel shows the magnetic field spatial scale, defined by $\lambda \equiv |\boldsymbol{B}|/|\nabla \times \boldsymbol{B}|$. Note that, as expected, higher grid resolution (and hence, higher magnetic Reynolds number) leads to smaller diffusive scales and larger field amplification.

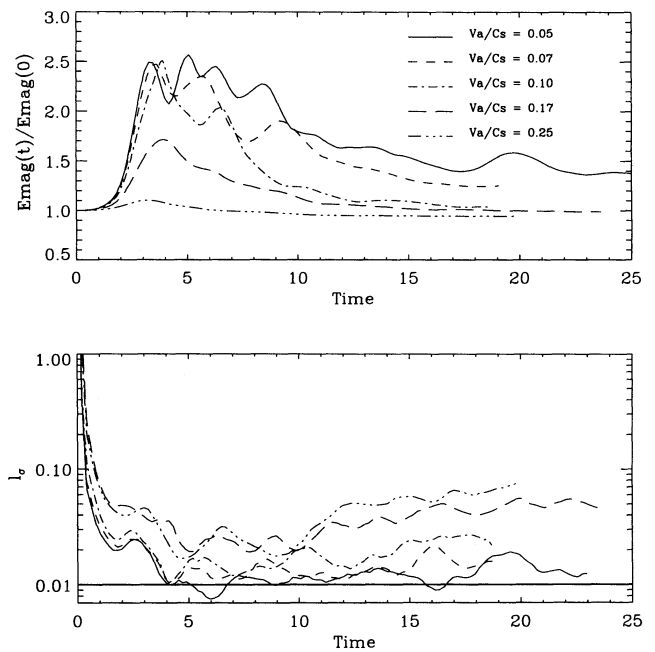

FIG. 6.—Magnetic field evolution as a function of time for different values of the initial magnetic energy, or $\alpha \equiv v_A/c_s$. The upper panel shows the averaged magnetic energy; the lower panel shows the magnetic field spatial scale, defined as in Fig. 5. The solid horizontal line in the lower panel indicates the value of the effective diffusive scale in these numerical computations. It is evident that field saturation occurs roughly when the spatial scale of the magnetic field reaches the diffusive scales. The temporal evolution of the magnetic field is not especially sensitive to α for very small values of α; however, for values of α larger than a critical value (here, roughly 0.1), there is a transition in which significant field amplification begins to be suppressed.

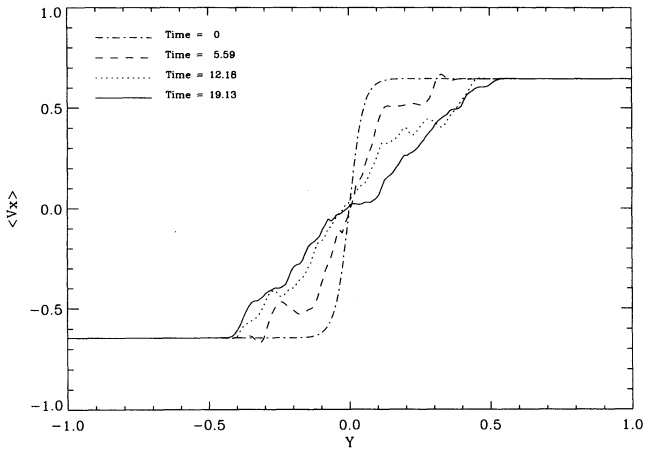

FIG. 7.—Temporal evolution of the velocity profile across the shear layer. It is evident that by $t \sim 12$ the velocity profile has relaxed to a quasi-steady form, which is basically stable against further disruption.

end of phase 1. We have verified this expectation by a simulation in which we perturbed both the fundamental wavelength ($ka \sim 0.05$) and its first harmonic ($ka \sim 0.1$); we find that vortex pairing occurs faster in phase 1, unimpeded by the presence of the magnetic field, so that, at the end of phase 1, we find only one big vortex remaining; the subsequent evolution is then the same as in the case where only one wavelength was perturbed.

Clearly, the largest wavelength that can be excited coincides with the Fourier mode corresponding to the horizontal size D of the computational domain. This is a consequence of our choice of periodic boundary conditions, which imposes a particular symmetry to the problem. However, it is clear that, as long as $D \gg a$, where a is the initial width of the shear layer as in equation (6), our results will scale in a self-similar way with D. Similarly, we can expect that if we embed the final quasi–steady state layer in a larger horizontal domain (by, for example, replicating the solution periodically), we would eventually find that the layer becomes unstable in the way pointed out by Ray (1986) (note that our final layer resembles closely his initial condition). A different choice of boundary conditions

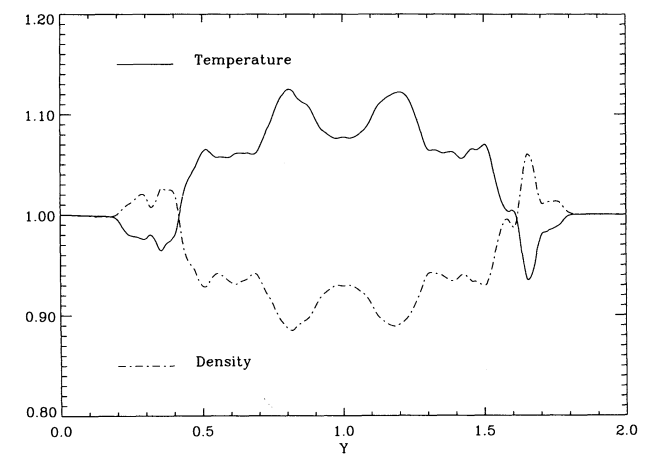

FIG. 8.—The average transverse profile of the temperature and density distribution across the layer at time $T = 19.1$ (same as in the rightmost panel in Fig. 1).

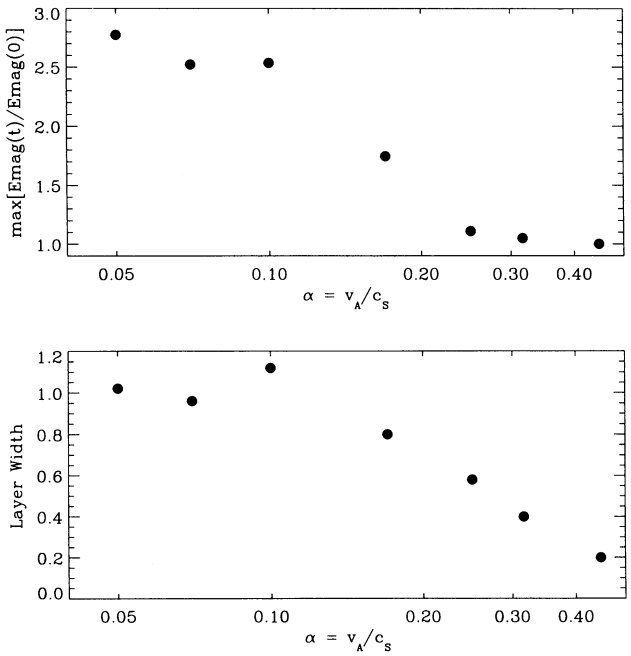

FIG. 9.—Maximum value of the magnetic energy attained (*upper panel*) and asymptotic mixed layer width (*lower panel*), as functions of the value of the initial Alfvén speed to sound speed ratio α.

may also produce different final results, like in the work of Wu (1986). More generally, more realistic models of specific astrophysical shear flows will be needed to determine the evolution of the Kelvin-Helmholtz instability in more realistic settings. However, such studies are beyond the scope of this beginning investigation into the nonlinear Kelvin-Helmholtz instability.

4. SUMMARY AND DISCUSSION

In this paper, we have used a new numerical method, based on the Godunov scheme, for integrating the single-fluid fully compressible magnetohydrodynamic equations to attack the nonlinear evolution problem for unstable magnetized shear flows. We have followed the (Kelvin-Helmholtz) shear flow instability well into the nonlinear regime, and we have discerned three stages in the instability's evolution: (i) a *linear* stage, in which exponential growth of the perturbed flow occurs, including that of the magnetic field perturbation; (ii)a *dissipative* transient stage, in which field amplification saturates and the ultimate decay of the strongly amplified fields begins via a succession of highly intermittent reconnection events; and (iii) a *saturation* stage, in which the small-scale turbulent motions decay to form aligned structures; the onset of this final stage is also signaled by the relaxation of the velocity profile to a statistically quasi-steady form.

The main result that emerges from our calculation is that even weak equilibrium magnetic fields can lead to a dramatic change in the instability evolution with respect to the purely hydrodynamical case. The reason is that the field is strongly amplified by the vortical motions that develop from the unstable modes growth and can become locally dynamically important. In such cases, it can then act as a mediator for the transfer of energy toward small scales, at which it can be quickly dissipated by localized reconnection events. This is very different from the pure hydrodynamical evolution, in which case energy is transferred to the largest scales, large vortices are formed, and dissipation is very ineffective. In this respect, an important parameter that can control the evolution is therefore the effective magnetic Reynolds number R_m. We have, in fact, explored the dependence of our results on R_m, showing that, as expected, larger R_m leads, in the first phase, to larger magnetic field amplification. By increasing the initial magnetic field strength, we determine how magnetic field amplification becomes gradually suppressed as the magnetic field approaches the critical intensity for which $\alpha = \alpha_c = 0.5$.

When the instability is active, the shear layer decays into an enlarged, steady vortex sheet in which the magnetic field returns approximately to its initial strength and orientation, while the flow material has been completely mixed and heated during the process of turbulence decay. The width of the final layer is enlarged from its initial state and is roughly equal to the size of the initial perturbation.

The very simple flow configuration we have studied here is obviously far removed from likely astrophysical situations. However, we have been able to identify some particular phenomena associated with the evolution of nonlinear magnetized Kelvin-Helmholtz instabilities, such as the dynamics of turbulence decay and associated energy dissipation mechanisms and material mixing, which are likely to play important roles in the more complex circumstances encountered in astrophysical systems.

A major unresolved issue is how our results are affected by dimensionality. That is, we would like to know what happens in three dimensions. A fundamental reason for believing that the problem in three dimensions may be significantly more complex is that dynamo action is then *not* prohibited; hence, it is not obvious that the strong fields built up during the linear phase 1 must subsequently decay in the three-dimensional case. Resolution of this issue is an obvious task for the future.

We would like to acknowledge partial support by the NASA Space Physics Theory Program and the NASA HPCC programs (A. M. and R. R). The computations were performed on the Cray YMP-8 at the National Center for Atmospheric Research. A. M. would like to thank A. Frank and T. W. Jones for carefully reading the manuscript and providing many useful comments to the authors.

REFERENCES

Artola, M., & Majda, A. 1988, J. Phys. D, 28, 253
———. 1989a, SIAM J. Appl. Math., 49, 1310
———. 1989b, Phys. Fluids A, 1, 583
Anzer, U., & Börner, G. 1983, ApJ, 122, 73
Bell, J. B., Colella, P., & Tragenstein, J. A. 1989, J. Chem. Phys., 82, 362
Birkinshaw, M. 1991a, Beams and Jets in Astrophysics, ed. P. A. Hughes (Cambridge: Cambridge Univ. Press), chap. 6
———. 1991b, MNRAS, 252, 505
Biskamp, D., & Welter, H. 1983, Phys. Fluids B, 1, 1964
Blumen, W., Drazin, P. G., & Billings, D. F. 1975, J. Fluid Mech., 71, 305
Bogdan, T. J., Cattaneo, F., & Malagoli, A. 1993, ApJ, 407, 316
Boris, J. 1991, private communication
Bührke, T., Mundt, R., & Ray, T. P. 1988, A&A, 200, 99
Chandrasekhar, S. 1961, Hydrodynamic and Hydromagnetic Stability (Oxford: Clarendon)
Colella, P., & Woodward, P. 1984, J. Chem. Phys., 54, 174
Fejer, J. A. 1964, Phys. Fluids, 7, 499
Ferrari, A., & Trussoni, E. 1983, MNRAS, 205, 515
Ferrari, A., Trussoni, E., & Zaninetti, L. 1980, MNRAS, 193, 469
———. 1981, MNRAS, 196, 1051
Frisch, U., Pouquet, A., Sulem, P.-L., & Meneguzzi, M. 1983, J. Méch. Theor. Appl., Numéro spécial, 191
Fryxell, B., Müller, E., & Arnett, D. 1991, ApJ, 367, 619
Gerwin, R. A. 1968, Rev. Mod. Phys., 40, 652

Hardee, P. E., Cooper, M. A., Norman, M. L., & Stone, J. M. 1992, ApJ, 399, 478
Lau, Y. Y., & Liu, C. S. 1980, Phys. Fluids, 23, 939
Lax, P. D. 1954, Comm. Pure Appl. Math., 7, 159
Lele, S. 1989, Direct Numerical Simulation of Compressible Free Shear Flows, AIAA Pap. 89, 0374
Malagoli, A., Cattaneo, F., & Brummell, N. H. 1991, ApJ, 361, L33
Miura, A. 1984, J. Geophys. Res., 89, 801
Miura, A., & Pritchett, P. L. 1982, J. Geophys. Res., 87, 1982
Moffatt, H. K. 1978, Magnetic Field Generation in Electrically Conducting Fluids (Cambridge: Cambridge University Press)
Orszag, S. A., & Tang, C. M. 1979, J. Fluid Mech., 90, 129
Picone, J. M., & Dahlburgh, R. B. 1991, Phys. Fluids B, 3, 29
Porter, D. H., Pouquet, A., & Woodward, P. R. 1994, Phys. Fluids, 6, 2133
Porter, D. H., & Woodward, P. R. 1994, ApJS, 93, 309
Pouquet, A. 1978, J. Fluid Mech., 88, 1
Pu, Z.-Y., & Kivelson, M. G. 1980, EOS Trans. AGU, 61, 1086
Pu, Z.-Y., & Kivelson, M. G. 1983, J. Geophys. Res., 88, 841
Ray, T. P. 1982, MNRAS, 198, 617
Sandham, N. D., & Reynolds, W. C. 1989, Rep. TF-45, Thermosciences Div., Mech. Eng. Dept., Stanford Univ.
———. 1991, J. Fluid Mech., 224, 133
Sen, A. K. 1963, Phys. Fluids, 6, 1154
———. 1964, Phys. Fluids, 7, 1293
Southwood, D. J. 1964, Planet. Space Sci., 16, 587
Talwar, S. P. 1964, J. Geophys. Res., 69, 2707
Trussoni, E., Massaglia, S., Bodo, G., & Ferrari, A. 1988, MNRAS, 234, 539
Uberoi, C. 1984, J. Geophys. Res., 89, 5652
Woodward, P. 1987, in Science and Engineering on Cray Supercomputers (Minneapolis: Cray)
Wu, C. C. 1986, J. Geophys. Res., 91, 3042
Zachary, A. L., Malagoli, A., & Colella, P. 1994, SIAM J. Sci. Stat. Comput., 15, 263